THE JOURNAL OF BIOLOGICAL CHEMISTRY VOL. 286, NO. 33, pp. 29356–29365, August 19, 2011

Cholesterol- and Sphingolipid-rich Microdomains Are Essential for Microtubule-based Membrane Protrusions Induced by *Clostridium difficile* Transferase (CDT)*

Received for publication, May 17, 2011, and in revised form, June 24, 2011 Published, JBC Papers in Press, June 25, 2011, DOI 10.1074/jbc.M111.261925

Carsten Schwan[1], **Thilo Nölke**[1], **Anna S. Kruppke, Daniel M. Schubert, Alexander E. Lang, and Klaus Aktories**[2]

From the Institut für Experimentelle und Klinische Pharmakologie und Toxikologie Albert-Ludwigs-Universität Freiburg, D-79104 Freiburg, Germany

Clostridium difficile **toxin (CDT) is a binary actin-ADP-ribosylating toxin that causes depolymerization of the actin cytoskeleton and formation of microtubule-based membrane protrusions, which are suggested to be involved in enhanced bacterial adhesion and colonization of hypervirulent *C. difficile* strains. Here, we studied the involvement of membrane lipid components of human colon adenocarcinoma (Caco-2) cells in formation of membrane protrusions. Depletion of cholesterol by methyl-β-cyclodextrin inhibited protrusion formation in a concentration-dependent manner but had no major effect on the toxin-catalyzed modification of actin in target cells. Repletion of cholesterol reconstituted formation of protrusions and increased velocity and total amount of protrusion formation. Methyl-β-cyclodextrin had no effect on the CDT-induced changes in the dynamics of microtubules. Formation of membrane protrusions was also inhibited by the cholesterol-binding polyene antibiotic nystatin. Degradation or inhibition of synthesis of sphingolipids by sphingomyelinase and myriocin, respectively, blocked CDT-induced protrusion formation. Benzyl alcohol, which increases membrane fluidity, prevented protrusion formation. CDT-induced membrane protrusions were stained by flotillin-2 and by the fluorescent-labeled lipid raft marker cholera toxin subunit B, which selectively interacts with GM1 ganglioside mainly located in lipid microdomains. The data suggest that formation and especially the initiation of CDT-induced microtubule-based membrane protrusions depend on cholesterol- and sphingolipid-rich lipid microdomains.**

Clostridium difficile causes antibiotic-associated diarrhea and pseudomembranous colitis (1). Both diseases depend on the production of toxins. Major virulence factors are the glycosylating *C. difficile* toxins A and B, which inactivate Rho GTPases (2–5). Especially hypervirulent strains additionally produce *C. difficile* transferase (CDT)[3] (6). CDT belongs to the family of actin-ADP-ribosylating toxins like *Clostridium perfringens* iota toxin and *Clostridium botulinum* C2 toxin (7–9). These toxins are binary in structure and consist of an enzymatic component, which possesses ADP-ribosyltransferase activity, and a separated binding/translocation component. The binding component is proteolytically activated and forms heptamers, which interact with the enzymatic component (8, 10). After binding of the toxin to a cell surface receptor, the toxin complex is endocytosed (11, 12). At low pH of endosomal compartments, the binding component inserts into the membrane of endosomes and forms pores, which allow the translocation of the enzymatic component into the cytosol (10, 13). Here, the toxin ADP-ribosylates actin at arginine 177 (14). Modification at this site inhibits actin polymerization and causes destruction of the actin cytoskeleton.

Recently, we reported that following ADP-ribosylation of actin, CDT induces the formation of microtubule-based protrusions in epithelial cells (15). These protrusions are in general <1 μm in diameter and have a variable length of 5–150 μm. They form a net on the surface of cells, which seems to facilitate adherence of bacteria and to increase colonization. Therefore, it has been suggested that CDT and related toxins increase pathogenicity at least partially by enhanced colonization (7, 15).

Toxin-induced formation of microtubule-based protrusions strictly depends on the redistribution of the actin cytoskeleton (15). However, the actin-ADP-ribosylating toxins do not only affect microtubule formation at the cell cortex but also inside the cells (16). In human leukemia HL-60 cells the actin-depolymerizing *C. botulinum* C2 toxin does not form major microtubule protrusions at the cell surface but largely increases formation of intracellular microtubules (16). Therefore, we aimed to characterize factors that are responsible for microtubule-based membrane protrusions. Here, we report that formation of toxin-induced microtubule protrusions depends on cholesterol and/or sphingomyelin content of membranes. Moreover, protrusion formation occurs at specific sites of the membrane that are enriched in ganglioside GM1. The data suggest that cholesterol- and sphingolipid-rich microdomains play a pivotal role in microtubule-based protrusions, which are induced by actin-ADP-ribosylating toxins.

EXPERIMENTAL PROCEDURES

Expression and Purification of Protein Toxins—The components of C2 toxin (C2I and C2II) were purified as described previously (10, 17). Recombinant CDTa and CDTb (from *C. difficile* strain 196) were produced as His-tagged proteins in the

* This work was supported by Deutsche Forschungsgemeinschaft Grant AK 6-20/1 and the BIOSS Program, Freiburg, Germany.

[1] Both authors contributed equally to this work.

[2] To whom correspondence should be addressed: Institut für Experimentelle und Klinische Pharmakologie und Toxikologie, Albert-Ludwigs-Universität Freiburg, Albertstr. 25, D-79104 Freiburg, Germany. Fax: 49-761-203-5311; E-mail: Klaus.Aktories@pharmakol.uni-freiburg.de.

[3] The abbreviations used are: CDT, *C. difficile* transferase; BA, benzyl alcohol; MβCD, methyl-β-cyclodextrin; Smase, sphingomyelinase; TRITC, tetramethylrhodamine-5-(and 6)-isothiocyanate.

Bacillus megaterium expression system as was described previously for the clostridial glycosylating toxins (18, 19). All binding components (CDTb and C2II) used in this study were used as protease-activated proteins according to Refs. 10, 17.

Cell Culture, Transient Transfection—Caco-2 cells were cultured in Dulbecco's modified Eagle's medium supplemented with 10% fetal calf serum (FCS), 1% nonessential amino acids, and 1% sodium pyruvate (Biochrom, Berlin, Germany). For immunostainings, cells were plated on HCl-washed coverslips. For live cell imaging, cells were plated on glass bottom dishes (Mattek, Ashland, MA). Cells were transfected using Lipofectamine 2000 (Invitrogen) or Attractene (Qiagen, Hilden, Germany) according to the manufacturers' protocols.

Antibodies and Fluorescent Dyes—Rabbit anti-Rab5 was from Santa Cruz Biotechnology (Santa Cruz, CA), and mouse monoclonal anti-α-tubulin and rabbit anti-flotillin-2 were from Sigma. All secondary Alexa568- and Alexa488-conjugated antibodies were purchased from Invitrogen. Actin was stained using phalloidin-TRITC (Invitrogen). GM1 was stained using fluorescein isothiocyanate (FITC)-conjugated cholera toxin subunit B (Sigma), and cholesterol was stained using filipin (Sigma).

Manipulation of Membrane Components—All drugs were purchased from Sigma. To extract cholesterol, Caco-2 cells were either plated on coverslips, culture dishes, or glass bottom dishes. Cells were plated at low density and incubated for 2–3 days. In the experiments, cells were still subconfluent. Cells were treated with 1–10 mM MβCD in buffer containing 10 mM HEPES (pH 7.5), 150 mM NaCl, 4 mM KCl, and 11 mM glucose for 30 min at 37 °C or after 30 min of CDT treatment when CDT had already entered cells. The same buffer was used for cholesterol repletion with water-soluble cholesterol (*e.g.* cholesterol balanced with MβCD). For treatment with the cholesterol-sequestering drug nystatin (20, 21), cells were incubated for 1 h at 37 °C with 25 μg/ml nystatin. For inhibition of glycosphingolipid synthesis, cells were treated with 10 μM myriocin for 48 h (22). For hydrolysis of sphingomyelin to ceramide and phosphorylcholine, cells were treated with 0.5 unit/ml of sphingomyelinase (Smase) from *Bacillus cereus* (23). For manipulation of membrane fluidity and to redistribute components of the liquid ordered phase, cells were treated with 40 mM benzyl alcohol (BA) after 45 min when CDT had already entered cells (24, 25).

Immunostaining—Cells were washed with warmed phosphate-buffered saline (PBS), fixed with 4% formaldehyde in PBS, washed again, and permeabilized with 0.15% Triton X-100 in PBS. Cells were blocked by 1% BSA and 0.05% Tween 20 in PBS for 30 min. Incubation with primary antibody was overnight at 4 °C in 1:200 (anti-flotillin-2, anti-Rab5) or 1:2000 (anti-α-tubulin) dilutions with the blocking solution. The samples were then washed with 0.05% Tween 20 in PBS and incubated with 1:200 dilutions of the secondary antibodies in blocking solution for 1.5 h at room temperature. Thereafter, cells were washed again and embedded with Mowiol supplemented with 1,4-diazobicyclo[2.2.2]octane (Sigma). For actin staining or GM1 staining, TRITC-conjugated phalloidin was diluted 1:200 from a 50 μg/ml stock solution together with the secondary antibody, and FITC-conjugated cholera toxin was diluted 10 μg/ml together with the secondary antibody. For cholesterol staining, cells were fixed and incubated with 50 μg/ml filipin (Sigma). Fixed samples were analyzed with an inverted Axiovert 200 M microscope (Carl Zeiss GmbH, Jena, Germany) equipped with plan-apochromat objectives, with a monochromator (Cairn Optoscan, Faversham Kent, UK) and suitable filters. Images were collected with a digital camera (Coolsnap HQ, Roper Scientific, Tucson, AZ) driven by Metamorph imaging software (Universal Imaging, Downingtown, PA). Confocal images were collected with a Yokogawa CSU-X1 spinning disc confocal head (Tokyo, Japan) with an emission filter wheel, a Coolsnap HQ II digital camera, with 488- and 561-nm laser lines.

Live Cell Imaging, Quantification of Formation of Protrusions, and Plus-end Tracking Protein (+TIP) Dynamics—For live cell imaging, cells were incubated in a chamber that provided a humidified atmosphere (6.5% CO_2 and 9% O_2) at 37 °C on a Zeiss Axiovert 200 M inverted microscope (Carl Zeiss GmbH, Jena, Germany). Differential interference contrast images were collected with a digital camera (Coolsnap HQ, Roper Scientific, Tucson, AZ) driven by Metamorph imaging software (Universal Imaging, Downingtown, PA). For the observation of protrusion formation, time-lapse series, lasting 2–3 h, were acquired with 60-s intervals. For quantification of formation of microtubule protrusions, the lengths of processes were summated every 15 min and normalized by the respective section of the cell perimeter that was accounted for analysis according to Ref. 15. Therefore, data in figures are given as "normalized formation of protrusions."

For the observation of +TIP dynamics, cells were transiently transfected with an EB3-GFP expression vector (kind gift of Dr. N. Galjart, Rotterdam, Netherlands) (26) and imaged 24–48 h after transfection. Time-lapse series of 3–4 min duration were acquired with a 2-s interval. Control cells were imaged, subsequently treated for 1.5 h, and imaged again. All quantifications were performed by the Metamorph software.

For the quantification of microtubule polymerization speed, steadily moving EB3-positive microtubule plus-ends were tracked for 10 s. The rate of polymerization was calculated from the covered distance during this time. For quantification of the time in growth, microtubules with EB3-GFP association at the tips of microtubules were recorded from their appearance until fading.

ADP-ribosylation Assays—For [^{32}P]ADP-ribosylation of nonmuscle actin (Cytoskeleton, Inc., Denver, CO), 2 μg of actin were incubated with [^{32}P]NAD and 500 ng of CDT at 37 °C for 30 min with or without MβCD. Proteins were subjected to SDS-PAGE, and radiolabeled actin was visualized by phosphorimaging. For "differential" ADP-ribosylation of lysates from Caco-2 cells, cells were lysed, and 30 μg of lysate protein were incubated for 30 min at 37 °C in the presence of [^{32}P]NAD and C2I toxin (enzymatic component) from *C. botulinum*. Proteins were also subjected to SDS-PAGE, and radiolabeled actin was visualized by phosphorimaging.

Statistics—Student's *t* test was applied, when two groups with normal distribution had to be compared. The Mann-Whitney *U* test was used for data without normal distribution. Statistical evaluation was performed with the SigmaStat soft-

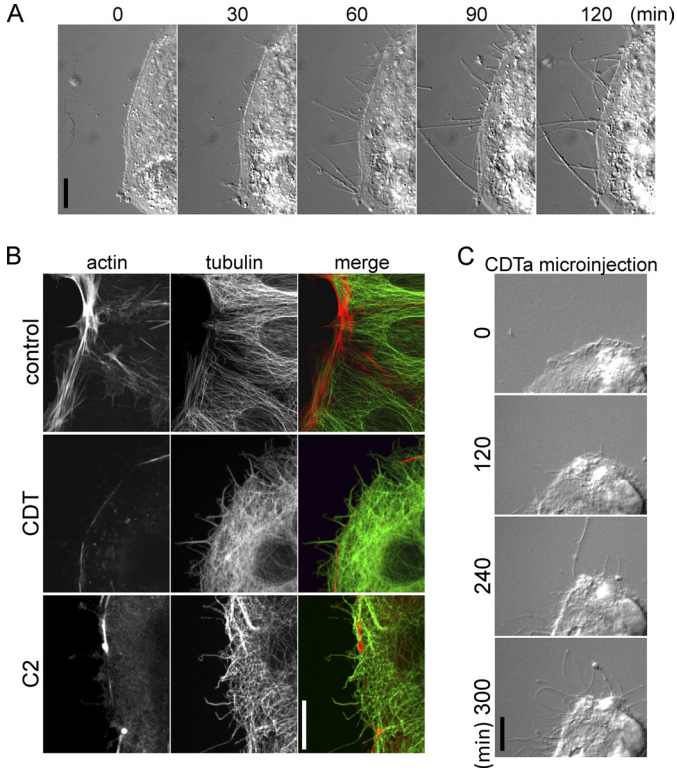

FIGURE 1. **Formation of protrusions.** *A,* subconfluent Caco-2 cells were treated with CDT (200 ng/ml CDTa and 400 ng/ml CDTb). In each panel the incubation time (min) is indicated. The *scale bar* represents 10 μm. *B,* indirect immunofluorescence of α-tubulin (*green*) and actin staining by TRITC-conjugated phalloidin (*red*) in Caco-2 cells is shown. Cells were treated with 200 ng/ml CDTa and 400 ng/ml CDTb or with *C. botulinum* C2 toxin (300 ng/ml C2I and 600 ng/ml C2II) for 1.5 h. The *calibration bar* represents 10 μm. *C,* Caco-2 cells were microinjected with 0.5 ng/ml CDTa and observed by time-lapse microscopy for the indicated times (min). *Scale bar,* 10 μm.

ware (Jandel Scientific, Corte Madera, CA). p values <0.05 were considered statistically significant and marked with an asterisk.

RESULTS

CDT-induced Cell Protrusions—Treatment of human colon carcinoma Caco-2 cells with CDT for up to 2 h caused formation of cellular protrusions in a time-dependent manner (Fig. 1*A*). Staining with rhodamine-phalloidin exhibited reduction of the actin cortical cytoskeleton after 1.5 h; concomitantly, cell protrusions appear that were stained by anti-tubulin antibody (Fig. 1*B*). A similar effect was observed with *C. botulinum* C2 toxin, which ADP-ribosylates actin at the same site (arginine 177), thereby inhibiting actin polymerization (27, 28). Next, the enzyme component CDTa was microinjected into Caco-2 cells without the binding component CDTb (Fig. 1*C*). For these studies, a low toxin concentration (10 pM) was used, and protrusion formation occurred after 4–5 h, indicating that the heptameric binding component CDTb is not involved in the molecular mechanism underlying formation of membrane protrusions.

Depletion of Cholesterol—To study the role of membrane lipids in CDT-induced protrusions, we analyzed the functional consequences of cholesterol depletion, which is a major constituent of biomembranes (29). MβCD is frequently employed to manipulate the cholesterol content of membranes (30–35). For cholesterol depletion of membranes, Caco-2 cells were treated with increasing concentrations of MβCD (Fig. 2, *A* and *B*). The depletion of cholesterol was verified by filipin staining (data not shown). Under control conditions the typical microtubule-based protrusions were observed. MβCD inhibited protrusion formation in a concentration-dependent manner. Addition of MβCD strongly decreased the number of protrusions formed, although the length of protrusions was less reduced (Fig. 2, *D* and *E*). Both parameters were taken together to quantify protrusion formation (Fig. 2*B*). At 1 mM MβCD, CDT-induced protrusion formation was reduced by ~60%. The cholesterol-depleting agent slightly increased the time lag until protrusion formation started, whereas the time to maximal protrusion formation was not affected. At 10 mM MβCD, protrusion formation was strongly inhibited. A similar inhibition of protrusion formation by MβCD was observed in the presence of the CDT-related C2 and iota toxins (data not shown). Notably, addition of MβCD caused changes in the morphology of cells. Formation of lamellipodia-like structures was observed. Because MβCD was added shortly before addition of the toxins, we tested whether the cholesterol-depleting agent had any effect on the uptake of the toxin. To this end, Caco-2 cells were treated for 1 and 2 h with the complete CDT toxin (CDTa plus CDTb) in the absence and presence of 5 mM MβCD. Thereafter, cells were lysed, and a differential ADP-ribosylation of actin was performed in cell lysate in presence of [^{32}P]NAD after addition of the enzymatic component of C2. Fig. 2*C* shows that CDT pretreatment of intact cells largely reduced [^{32}P]ADP-ribosylation of actin in cell lysates in a time-dependent manner, indicating modification of actin in intact cells. Treatment of cells with MβCD slightly decreased the modification of actin *in vivo*. This effect was maximal after 1 h of CDT treatment and was hardly observable after 2 h. Considering the finding that MβCD strongly blocked formation of microtubule-based protrusion but had only minor effects on the time course of ADP-ribosylation of actin, we concluded that any effects of MβCD on the toxin uptake process are not responsible for inhibition of protrusion formation. This notion was supported by the finding that addition of toxins before MβCD treatment did not change the inhibition of protrusion formation (Fig. 3*B*) and gave a similar result in ADP-ribosylation as shown in Fig. 2*C* (Fig. 3*C*). Additionally, Alexa568-labeled CDTa was still found in Rab5-positive vesicles (data not shown), and MβCD had no effect on ADP-ribosylation of purified actin *in vitro* (data not shown).

Repletion of Cholesterol—Next, we studied the effects of cholesterol replenishment on toxin-induced formation of cell protrusions. As shown in Fig. 3*A*, when cholesterol was re-added, a rapid formation of protrusions occurred in previously cholesterol-depleted cells. The formation of protrusions after cholesterol repletion was ~2-fold faster than under control conditions (Fig. 3*B*).

Immunofluorescence Studies after Cholesterol Depletion—To study the effects of MβCD on the actin cytoskeleton and the microtubule system in detail, we employed immunofluorescence microscopy. In the absence of MβCD, CDT caused depolymerization of the cortical actin and strong formation of microtubule-based protrusions (Fig. 4*A*). As reported recently,

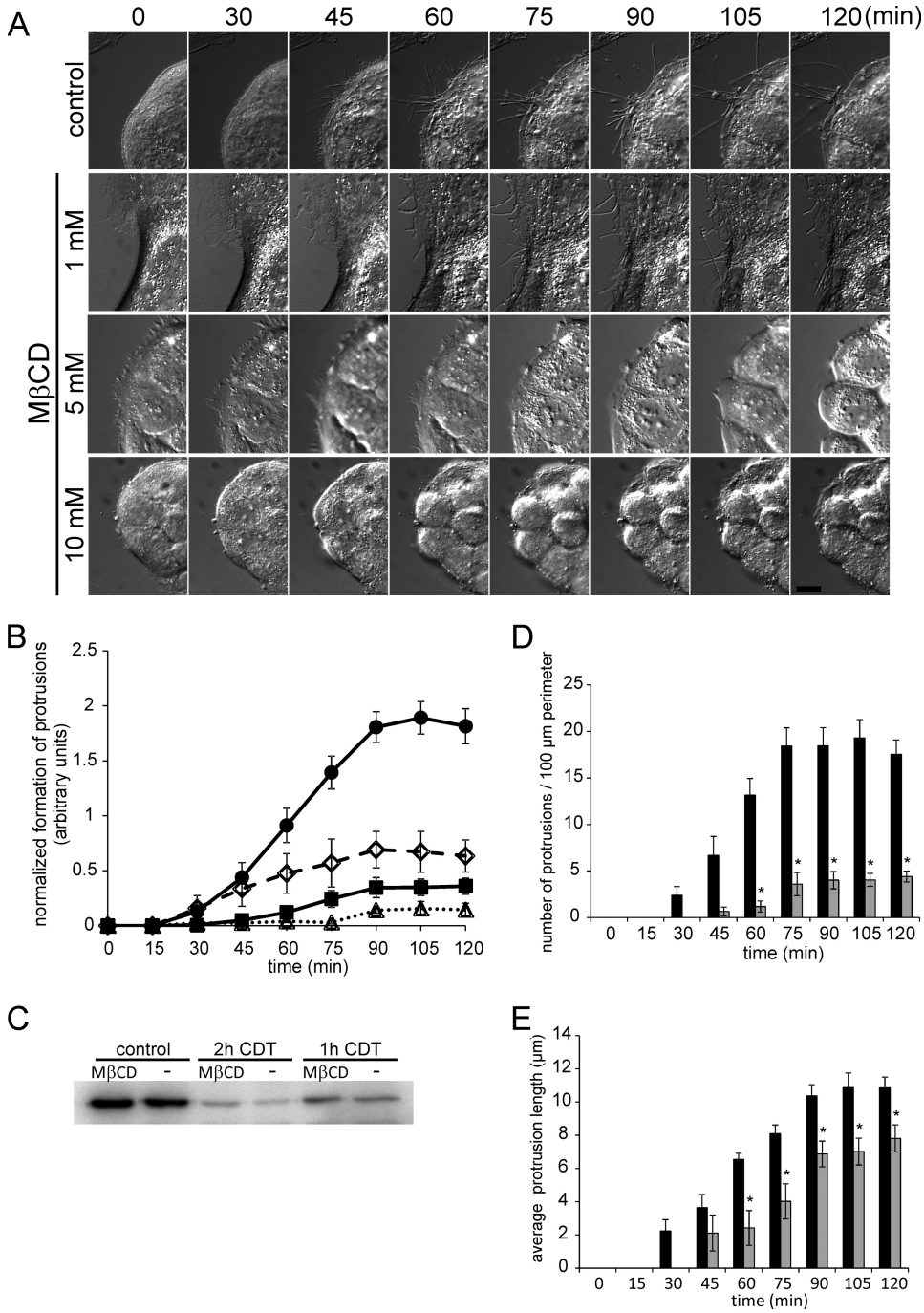

FIGURE 2. **Formation of protrusions is inhibited by cholesterol depletion.** *A,* subconfluent Caco-2 cells were pretreated with increasing concentrations of MβCD for 30 min or left untreated. Subsequently, all cells were treated with 200 ng/ml CDTa and 400 ng/ml CDTb. In each panel the incubation time (min) and the MβCD concentration are indicated. *Scale bar,* 10 μm. *B,* quantification of formation of protrusions. The lengths of all processes of cells were summated every 15 min after addition of the toxins and normalized by the respective section of the cell perimeter. Cells were treated as in *A* (control, CDT only, *solid line*, ●; 1 mM MβCD, *dashed line*, ◇; 5 mM MβCD, *solid line*, ■; 10 mM MβCD, *dotted line*, △). Increasing concentrations of MβCD slightly delayed the formation of protrusions and strongly reduced the formation of protrusions. Data are given ±S.E. from $n \geq 5$ movies and at least two cells per movie. *C, in vitro* [^{32}P]ADP-ribosylation of actin by the enzyme component C2I after intracellular ADP-ribosylation by CDT. Caco-2 cells were treated with 200 ng/ml CDTa and 400 ng/ml CDTb for 1 or 2 h with or without an additional pretreatment with 5 mM MβCD for 30 min. Cells were lysed after 1 or 2 h, and unmodified actin was subsequently modified by C2I in the presence of [^{32}P]NAD. The [^{32}P]ADP-ribosylated actin was analyzed by SDS-PAGE and phosphorimaging. The autoradiogram of an ADP-ribosylation from a representative experiment is shown. *D,* subconfluent Caco-2 cells were pretreated with 5 mM MβCD for 30 min (*gray boxes*) or left untreated (*black boxes*) and subsequently treated with 200 ng/ml CDTa and 400 ng/ml CDTb. The incubation time (min) is indicated. The number of protrusions per 100-μm cell perimeter was counted. Data are given ± S.E. from $n \geq 5$ movies and at least two cells per movie. *E,* quantification of the average length of protrusions. Cells were treated as in *D*. Data are given ±S.E. from $n \geq 5$ movies and at least two cells per movie. * = $p < 0.05$.

these protrusions occurred exclusively at sites where the actin cortex was diminished (15). When MβCD was added, protrusion formation was blocked, although the cortical actin cytoskeleton was depolymerized by CDT. However, the formation of microtubules, measured by intensity of fluorescence, appeared to be increased (note the velocity of polymerization is

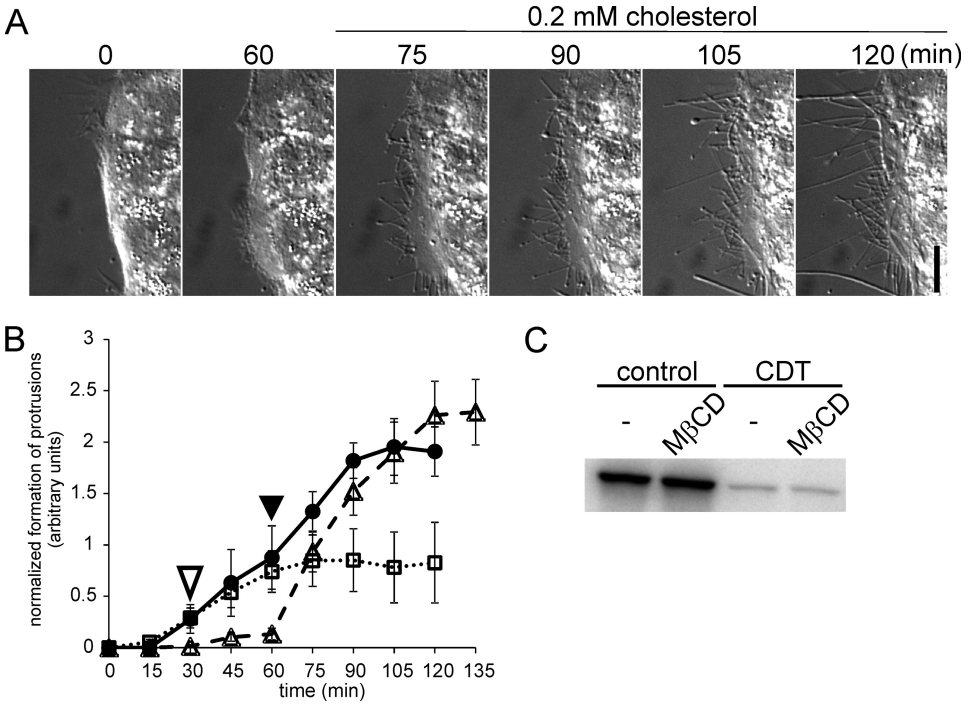

FIGURE 3. **Formation of protrusions is inhibited by cholesterol depletion and restored by cholesterol repletion.** *A,* subconfluent Caco-2 cells were pretreated with 5 mM MβCD for 30 min and subsequently treated with CDT (200 ng/ml CDTa and 400 ng/ml CDTb). After 60 min, medium was replaced by a buffer containing 0.2 mM water-soluble cholesterol. In each panel the incubation time (min) is indicated. *Scale bar,* 10 μm. *B,* quantification of formation of protrusions over time. Cells were treated with CDT (as in *A*, *dashed line*, △), treated only with CDT in the absence of MβCD (*solid line*, ●), or first treated with CDT and 5 mM MβCD were added (*open arrowhead*) after 30 min (*dotted line*, □) when first protrusions were formed. Repletion of cholesterol (*filled arrowhead*) caused a fast formation of protrusions. Data are given ±S.E. from $n \geq 5$ movies and at least two cells per movie. *C, in vitro* [^{32}P]ADP-ribosylation of actin by the enzyme component C2I in lysates of Caco-2 cells that were first pretreated with CDT (200 ng/ml CDTa and 400 ng/ml CDTb for 2 h) and subsequently treated with or without 5 mM MβCD (similar to *B*, *dotted line*, □). Cells were lysed after 2 h, and unmodified actin was subsequently modified by C2I in the presence of [^{32}P]NAD. The [^{32}P]ADP-ribosylated actin was analyzed by SDS-PAGE and phosphorimaging. A representative autoradiogram is shown.

reduced; see below). Particularly in submembranous areas, CDT caused enhanced microtubule formation and bundling (Fig. 4*A*). Comparison of the fluorescence intensity of microtubule staining in this area revealed that MβCD increased microtubule density above the high level already observed after CDT treatment (Fig. 4*B*). Detailed microscopic analyses showed that many microtubules were bending in the presence of MβCD (Fig. 4*A*, *mag.*), when they reached the cell membrane and were directed back into the interior of the cell. Cholesterol repletion by the addition of water-soluble cholesterol (*e.g.* cholesterol balanced with MβCD) caused rapid formation of microtubule-based protrusions.

Because MβCD influenced microtubule density and distribution, we studied its effects on microtubule dynamics by EB3-GFP comet tracking (Fig. 5). Recently, we reported that the destruction of the actin cytoskeleton by CDT causes changes in the polymerization behavior of microtubules (15). CDT was shown to reduce the velocity of microtubule growth, although the plus-end tips are longer in the growth state as compared with controls. Here, these data were confirmed. Moreover, treatment of cells with 5 mM MβCD did not change the effects of CDT on tubulin dynamics. Thus, the effect of MβCD on CDT-induced protrusion formation cannot be explained by changes in the polymerization behavior of microtubules but rather appears to be caused by MβCD-induced changes of membrane properties.

Lipid Microdomains Are Involved in Protrusion Formation—Cholesterol is considered to be a main part of a membrane microdomain termed liquid ordered phase or lipid rafts (36–39). Another component of this membrane microdomain is sphingomyelin (36, 38, 40). Therefore, we studied whether the destruction of sphingomyelin by sphingomyelinase has any effects on CDT-induced microtubule-based protrusions. Treatment of Caco-2 cells with sphingomyelinase from *B. cereus* for 1 h strongly reduced subsequent CDT-induced protrusion formation (Fig. 6*A*). The quantification of the experiment exhibited an ~60% inhibition of protrusion formation by sphingomyelinase (Fig. 6*B*). This treatment had no major effect on CDT uptake, because actin was ADP-ribosylated to the same extent with and without pretreatment of cells with sphingomyelinase (Fig. 6*C*).

The polyene antibiotic nystatin, which binds to cholesterol, is another lipid raft perturbating agent (20, 21). Fig. 6*B* shows that nystatin inhibited CDT-induced formation of protrusions in a manner similar to sphingomyelinase. Next, we studied the effects of myriocin, an inhibitor of serine palmitoyltransferase that causes depletion of sphingolipids and affects raft formation (41). Also myriocin inhibited formation of CDT-induced protrusions (Fig. 6*B*). Cell survival was not affected by myriocin during the treatment period (data not shown).

Finally, we employed BA as an agent, which is known to increase membrane fluidity and to redistribute components of the liquid ordered phase (24, 25). For this purpose, cells were treated with CDT until formation of the first small protrusions was observed, and BA (40 mM) was then added. Almost imme-

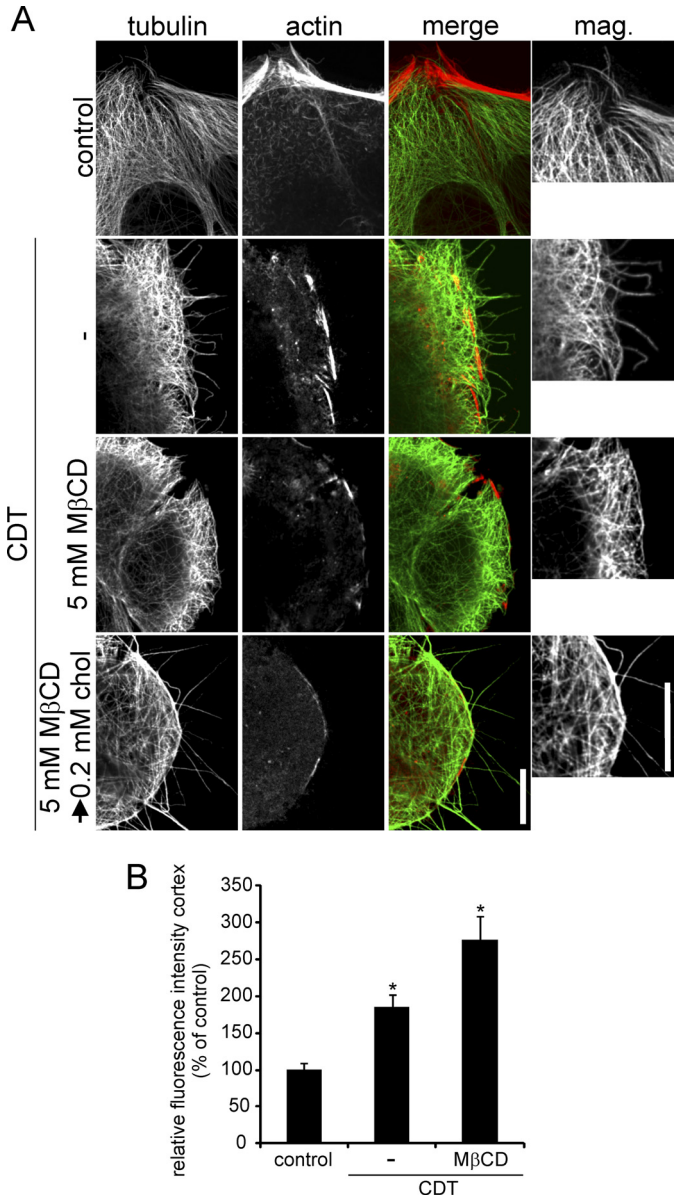

FIGURE 4. **Microtubule behavior at the cell cortex.** *A,* indirect immunofluorescence of α-tubulin (*green*) and actin staining by TRITC-conjugated phalloidin (*red*) in Caco-2 cells. Cells were treated with 200 ng/ml CDTa and 400 ng/ml CDTb for 1.5 h or additionally pretreated with 5 mM MβCD to deplete cholesterol or the cells were repleted with 0.2 mM water-soluble cholesterol after cholesterol depletion or left untreated. *B,* to estimate microtubule density at the cell cortex, fluorescence intensity was measured in an area reaching 5 μm from the cell cortex to the cell interior. Cells were treated as in *A*. CDT increases microtubule density at the cell cortex. (*A*, magnifications, *2nd row, 4th column*). In cholesterol-depleted cells bending of microtubules is increased resulting in higher fluorescence and microtubule density (*A*, magnifications, *3rd row, 4th column*). *Scale bar,* 10 μm; * = $p < 0.05$.

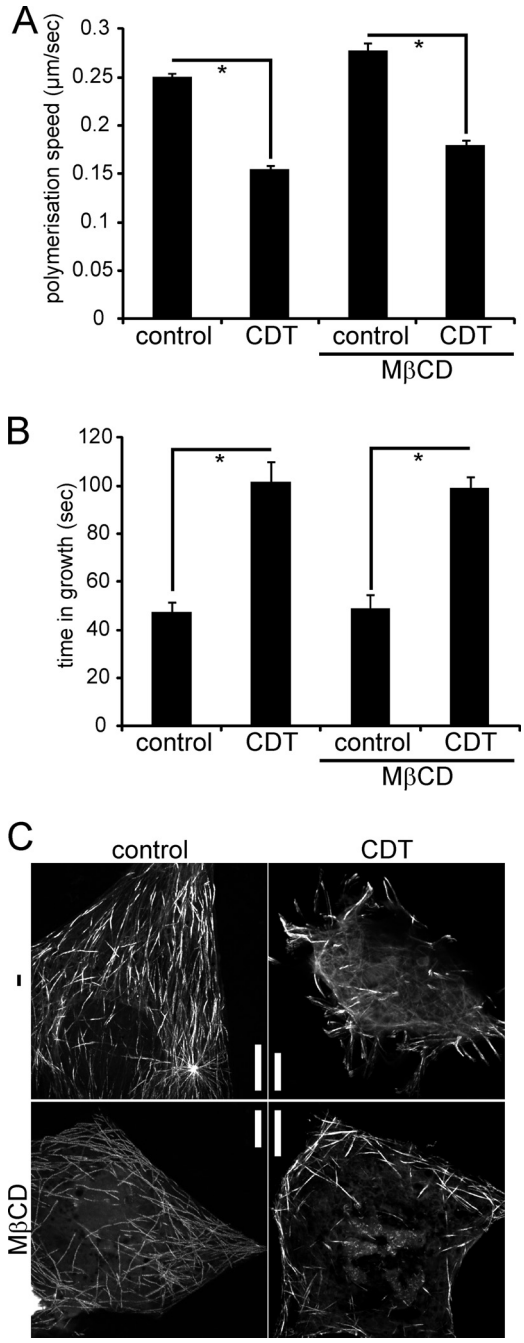

FIGURE 5. **Microtubule polymerization in CDT- and MβCD-treated cells.** Caco-2 cells transfected with EB3-GFP were monitored in fluorescence time-lapse microscopy. Cells were recorded 1.5 h after treatment with CDT (200 ng/ml CDTa and 400 ng/ml CDTb) or with an additional pretreatment with 5 mM MβCD. *A,* quantification of microtubule polymerization rate. Growing microtubules (EB3-GFP comets) were tracked over 10 s after CDT treatment. Data from ≥50 comets (five experiments) are given ±S.E. *B,* quantification of microtubule time in growth. The lifetime of ≥25 EB3-GFP comets from appearance to fading was measured (data are given ±S.E., ≥4 independent experiments). *C,* projections of EB3-GFP time-lapse microscopy. Images from 3 min movies (one picture every 3 s) were projected in one image to show tracks of polymerizing microtubules (treated as in *A* and *B*). In control cells, microtubules polymerize equally in the cell to form an ordered microtubule array. In CDT-treated cells, polymerization occurs mainly at the cell cortex and in formed protrusions. In MβCD-treated cells, microtubule polymerization takes place in the entire cell similar to control cells. In MβCD and CDT-treated cells, microtubules mainly polymerize at the cell cortex but without the formation of processes.

diately, the formation of typical protrusions was stopped (Fig. 6*D*).

BA did not cause a major decrease in cell survival measured by CellTiter Blue Cell Viability Assay (Promega, Madison, WI) (data not shown). As all these pharmacological tools suggested that lipid microdomains, containing cholesterol and sphingolipids, are essential for CDT-induced microtubule-based cell protrusions, we analyzed the localization of the lipid raft marker ganglioside GM1 by FITC-conjugated cholera toxin subunit B during formation of membrane protrusions (Fig. 7)

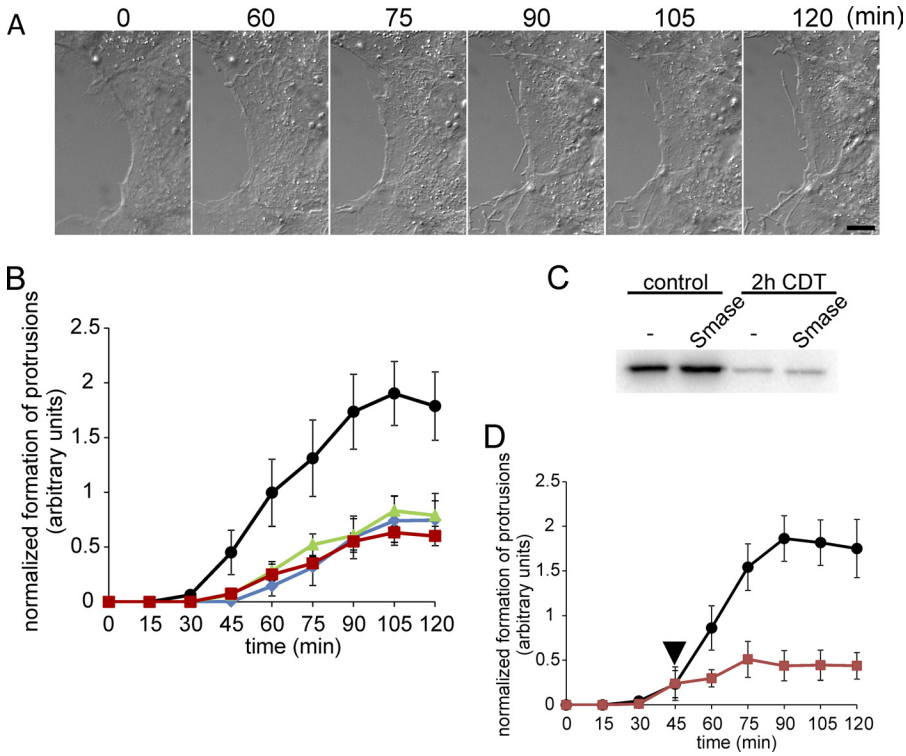

FIGURE 6. **Formation of protrusions is inhibited by Smase, myriocin, and nystatin.** *A,* subconfluent Caco-2 cells were pretreated with 0.5 units/ml Smase for 1 h and subsequently cells were treated with CDT (200 ng/ml CDTa and 400 ng/ml CDTb). In each panel the incubation time (min) is indicated. *Scale bar,* 10 μm. *B,* quantification of formation of protrusions. The lengths of all processes of cells were summated every 15 min after addition of the toxins and normalized by the respective section of the cell perimeter. Cells were pretreated with 0.5 unit/ml Smase for 1 h (■, *red*), with 10 μM myriocin for 48 h (▲, *green*), with 25 μg/ml nystatin for 1 h (◆, *blue*), or left untreated (●, *black*). Subsequently, cells were treated with CDT (200 ng/ml CDTa and 400 ng/ml CDTb). Data are given ±S.E. from $n \geq 5$ movies and at least two cells per movie. *C, in vitro* [^{32}P]ADP-ribosylation of actin by the enzyme component C2I in lysates of Caco-2 cells that were pretreated with CDT (200 ng/ml CDTa and 400 ng/ml CDTb for 2 h) with or without an additional pretreatment with 0.5 unit/ml Smase for 1 h. Cells were lysed after 2 h, and unmodified actin was subsequently modified by C2I in the presence of [^{32}P]NAD. The [^{32}P]ADP-ribosylated proteins were analyzed by SDS-PAGE and phosphorimaging (shown). *D,* quantification of formation of protrusions after BA treatment. Cells were treated with CDT (200 ng/ml CDTa and 400 ng/ml CDTb). After 45 min when first protrusions were formed, cells were additionally treated with 40 mM BA (*red square*; BA addition is indicated by *black arrowhead*) or left untreated (*black circle*). Data are given ±S.E. from $n \geq 5$ movies and at least two cells per movie.

(42). Fluorescence microscopic studies revealed that GM1 binding was observed all over the cell membranes of control cells. Interestingly, labeling with the FITC-conjugated cholera toxin subunit B appeared to be enhanced at membrane sites, from which formation of toxin-induced protrusions occurred, indicating specific localization of the membrane, which are prone to protrusion formation. In particular, the tips of protrusions, which often exhibited balloon-like structures, were intensively stained by the GM1 marker. Similar results were obtained with the lipid raft marker flotillin-2 (43) (data not shown). Microtubule-based protrusions and the site of formation were enriched in flotillin-2. Thus, all the data indicate that microdomains of liquid ordered phases or lipid rafts play a pivotal role in microtubule-based protrusion formation.

DISCUSSION

Recently, we observed that depolymerization of the actin cytoskeleton by the ADP-ribosylation of actin at arginine 177 induces the formation of long cell protrusions, containing microtubules (15). This type of protrusions, which build a tentacle-like network of processes on the cell surface, increase adhesion and probably colonization of the toxin-producing bacteria (15). Here, we analyzed the role of membrane constituents in protrusion formation. We report that cholesterol is essential for formation of CDT-induced protrusions. Cholesterol depletion by MβCD inhibited protrusion formation in a concentration-dependent manner. Moreover, inhibition of protrusion formation by MβCD was not caused by blockade of the toxin uptake because differential ADP-ribosylation experiments revealed that actin was modified in intact cells after cholesterol depletion. We observed that MβCD slightly delayed the uptake of the toxin, indicating a possible role of cholesterol in toxin-induced pore formation or translocation. However, this minor effect did not prevent complete modification of cellular actin. Also, *in vitro* studies revealed that MβCD (1–10 mM) did not inhibit actin ADP-ribosylation.

It has been shown that treatment of cells with CDT induces a decreased velocity in polymerization of tubulin and a prolonged time in growth of microtubules (15). Depletion of cholesterol did not change these effects of CDT on microtubule dynamics. Thus, inhibition of protrusion formation by cholesterol is most likely not caused by a direct effect on microtubules or microtubule dynamics but rather by changes in the biophysical properties of the membrane. It is of note that cholesterol depletion mainly reduced the number of CDT-induced protrusions formed, although the growth of protrusion was less affected. Therefore, it is suggested that cholesterol is mainly important for the initiation of protrusion formation.

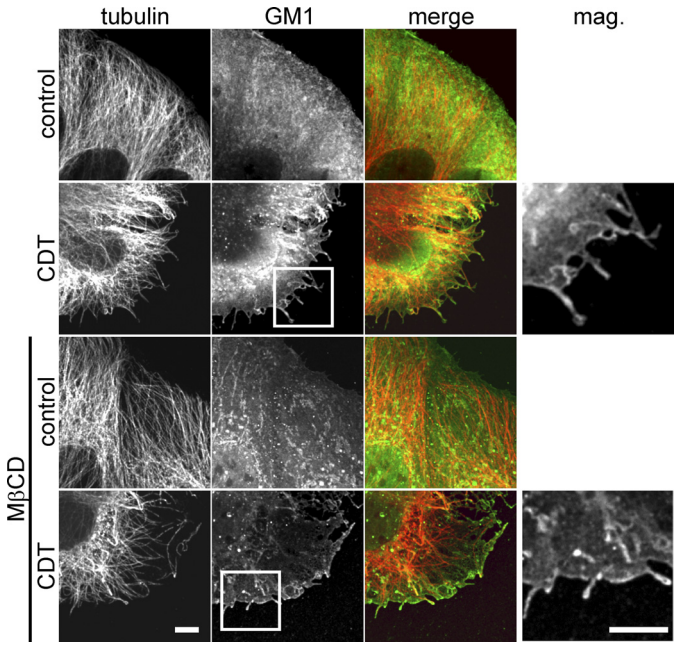

FIGURE 7. **Microtubule-based protrusions and the site of their formation are enriched in ganglioside GM1.** Indirect immunofluorescence of α-tubulin (*red*) and GM1 staining by FITC-conjugated cholera toxin subunit B (*green*) in Caco-2 cells are shown. Cells were treated with 200 ng/ml CDTa and 400 ng/ml CDTb for 1.5 h or additionally pretreated with 5 mM MβCD to deplete cholesterol. Protrusions are labeled with cholera toxin. MβCD-treated cells form much less protrusions. The residual protrusions still have increased levels of GM1. *Scale bars,* 5 μm.

To exclude unspecific effects of MβCD not related to cholesterol depletion (44), we repleted cholesterol after MβCD treatment. Repletion of cholesterol resulted in rapid formation of CDT-induced protrusions. The delay in formation of microtubule-based protrusions after treatment of target cells with CDT is probably caused by the time needed for toxin uptake. Therefore, it is not surprising that after repletion of cholesterol the formation of CDT-induced protrusions started earlier than under control conditions. However, the velocity of protrusion formation was increased. Moreover, the total amount of protrusion formation (estimated as number and length of protrusions) was increased after cholesterol repletion. In particular, the kinetics of protrusion formation after readdition of cholesterol indicate that cholesterol plays a specific and essential role in formation of membrane protrusions. In line with the results obtained with MβCD, we observed inhibition of protrusion formation by addition of the polyene antibiotic nystatin, which is known to sequester cholesterol (20, 21).

Cholesterol together with sphingolipids are the main components of lipid microdomains (36–39), also called liquid ordered phase, detergent-resistant membrane microdomains, or lipid rafts. These membrane structures have been frequently implicated in membrane curvature, tubule formation, budding, and fission (45). Besides the essential role of cholesterol, several additional findings indicate that these microdomains play a pivotal role in CDT-induced protrusion formation. First, sphingomyelinase, which metabolizes sphingolipids to ceramide and phosphorylcholine (23), blocked protrusion formation. Second, myriocin, a serine palmitoyltransferase inhibitor that blocks sphingosine biosynthesis (41), efficiently reduced protrusion formation caused by CDT. Finally, benzyl alcohol, which increases the fluidity of membranes and destroys lipid rafts (24, 25), strongly inhibited protrusion formation.

We also tested the role of lipid microdomains in protrusion formation by using lipid raft markers. The ganglioside GM1 is located at lipid rafts, and this glycolipid can be selectively stained by FITC-labeled cholera toxin B subunit (42). Our results showed that CDT-induced protrusions were frequently stained by FITC-conjugated cholera toxin subunit B. Moreover, initiation of protrusion formation appeared to occur at membrane sites, which were labeled by FITC-conjugated cholera toxin subunit B. Similarly, flotillin-2, another raft marker (43), caused strong labeling of protrusions.

Membrane curvature and protrusion formation depends on a complex interplay between membrane lipids, integral and peripheral membrane proteins, and physical forces (45, 46). Vesicle formation by different types of endocytosis, involving a large array of essential proteins, have been described in detail (for review see Refs. 47, 48), and clathrin-independent tubule invagination was studied recently (49–51). Formation of membrane processes like filopodia directed to the outside of cells has been described in detail with actin-based structures (52, 53). Moreover, a function of actin in regulation of membrane tubules induced by Shiga toxin has been reported (50). However, CDT induces formation of cell protrusions, which depends on microtubule structures. Although it is clear that destruction of the actin cytoskeleton is a prerequisite for CDT-induced formation of membrane protrusions, the precise molecular mechanism of microtubule-based protrusion formation is not well understood. Recently, we reported that CDT causes redistribution of the microtubule capture proteins CLASP2 and ACF7 from the membrane cortex to the interior of cells most likely by destruction of the actin cytoskeleton (15). Thus, by dislocation of these capture proteins, regulation of microtubules is altered and microtubule growth might persist. In addition, formation of protrusions appear to depend on the presence of specific sites of the membrane, which are similar to the above described lipid microdomains or lipid rafts. Therefore, the following question remains. What is the mechanism by which these membrane domains allow formation of protrusions?

The globotriaosyl ceramide-interacting pentavalent binding component of Shiga toxin is known to induce tubular invagination by a mechanism that involves glycolipid clustering (49). Similar findings have been reported for the GM1-interacting cholera toxin (54) and for Simian virus 40 (SV40) (55, 56). The binding component of CDT forms heptameric structures. To exclude that multivalent binding to an unknown receptor might cause clustering of glycolipids or membrane proteins, resulting in membrane tubule formation, we studied the effects of microinjection of the enzyme component CDTa in the absence of the binding component CDTb into target cells. Microinjected CDTa (without CDTb) induced protrusions, indicating that CDTb-induced clustering at the cell surface is not necessary for protrusion formation. Noteworthy, formation of membrane invaginations by polyvalent binding components

of toxins like Shiga toxin are reportedly not dependent on cholesterol (50), indicating a different molecular mechanism.

Cholesterol is essential for vesicle traffic to cell membranes and apical sorting (32). Moreover, studies with artificial membranes showed that lipid microdomains may induce membrane curvature and tubule formation simply by steric confinement of proteins (57). Thus, it is feasible that cholesterol depletion inhibits transport of proteins (or of other membrane constituents), which are essential for tubule formation. Moreover, it remains to be studied whether cholesterol depletion has any effects on signaling (*e.g.* change of the activity of protein kinases), which has been reported by others (58). Changes in signaling might be important for regulation of microtubule dynamics.

Taken together, cholesterol and sphingolipid-rich microdomains are essential for CDT-induced microtubule-based protrusions. Our data indicate that not only the actin cytoskeleton but also microtubules tightly interact with these structures. So far it is not clear which molecular mechanisms are involved in the interaction of microtubules with lipid microdomains, resulting in protrusion formation. However, at least force generation caused by tubulin polymerization or microtubule motor proteins and specific clustering of lipid-interacting proteins at the tip of microtubules are important options, which have to be studied in the future.

Acknowledgments—We thank Elke Heitzmann, Antje Müller, and Gerhard Wetterer for technical assistance.

REFERENCES

1. Kelly, C. P., and LaMont, J. T. (2008) *N. Engl. J. Med.* **359,** 1932–1940
2. Just, I., and Gerhard, R. (2004) *Rev. Physiol. Biochem. Pharmacol.* **152,** 23–47
3. Voth, D. E., and Ballard, J. D. (2005) *Clin. Microbiol. Rev.* **18,** 247–263
4. Jank, T., and Aktories, K. (2008) *Trends Microbiol.* **16,** 222–229
5. Davies, A. H., Roberts, A. K., Shone, C. C., and Acharya, K. R. (2011) *Biochem. J.* **436,** 517–526
6. Warny, M., Pepin, J., Fang, A., Killgore, G., Thompson, A., Brazier, J., Frost, E., and McDonald, L. C. (2005) *Lancet* **366,** 1079–1084
7. Aktories, K., Lang, A. E., Schwan, C., and Mannherz, H. G. (2011) *FEBS J.* doi: 10.1111/j.1742–4658.2011.08113.x
8. Barth, H., Aktories, K., Popoff, M. R., and Stiles, B. G. (2004) *Microbiol. Mol. Biol. Rev.* **68,** 373–402
9. Barbieri, J. T., Riese, M. J., and Aktories, K. (2002) *Annu. Rev. Cell Dev. Biol.* **18,** 315–344
10. Barth, H., Blocker, D., Behlke, J., Bergsma-Schutter, W., Brisson, A., Benz, R., and Aktories, K. (2000) *J. Biol. Chem.* **275,** 18704–18711
11. Pust, S., Barth, H., and Sandvig, K. (2010) *Cell. Microbiol.* **12,** 1809–1820
12. Gibert, M., Monier, M. N., Ruez, R., Hale, M. L., Stiles, B. G., Benmerah, A., Johannes, L., Lamaze, C., and Popoff, M. R. (2011) *Cell. Microbiol.* **13,** 154–170
13. Schmid, A., Benz, R., Just, I., and Aktories, K. (1994) *J. Biol. Chem.* **269,** 16706–16711
14. Gülke, I., Pfeifer, G., Liese, J., Fritz, M., Hofmann, F., Aktories, K., and Barth, H. (2001) *Infect. Immun.* **69,** 6004–6011
15. Schwan, C., Stecher, B., Tzivelekidis, T., van Ham, M., Rohde, M., Hardt, W. D., Wehland, J., and Aktories, K. (2009) *PLoS Pathog.* **5,** e1000626
16. Uematsu, Y., Kogo, Y., and Ohishi, I. (2007) *Biol. Cell* **99,** 141–150
17. Sterthoff, C., Lang, A. E., Schwan, C., Tauch, A., and Aktories, K. (2010) *Infect. Immun.* **78,** 1468–1474
18. Yang, G., Zhou, B., Wang, J., He, X., Sun, X., Nie, W., Tzipori, S., and Feng, H. (2008) *BMC Microbiol.* **8,** 192
19. Papatheodorou, P., Zamboglou, C., Genisyuerek, S., Guttenberg, G., and Aktories, K. (2010) *PLoS One* **5,** e10673
20. Pietiäinen, V., Marjomäki, V., Upla, P., Pelkmans, L., Helenius, A., and Hyypiä, T. (2004) *Mol. Biol. Cell* **15,** 4911–4925
21. Simons, K., and Toomre, D. (2000) *Nat. Rev. Mol. Cell Biol.* **1,** 31–39
22. Poole, K., Meder, D., Simons, K., and Müller, D. (2004) *FEBS Lett.* **565,** 53–58
23. Ikezawa, H., Mori, M., Ohyabu, T., and Taguchi, R. (1978) *Biochim. Biophys. Acta* **528,** 247–256
24. Nagy, E., Balogi, Z., Gombos, I., Akerfelt, M., Björkbom, A., Balogh, G., Török, Z., Maslyanko, A., Fiszer-Kierzkowska, A., Lisowska, K., Slotte, P. J., Sistonen, L., Horváth, I., and Vígh, L. (2007) *Proc. Natl. Acad. Sci. U.S.A.* **104,** 7945–7950
25. Bassé, F., Sainte-Marie, J., Maurin, L., and Bienvenüe, A. (1992) *Eur. J. Biochem.* **205,** 155–162
26. Stepanova, T., Slemmer, J., Hoogenraad, C. C., Lansbergen, G., Dortland, B., De Zeeuw, C. I., Grosveld, F., van Cappellen, G., Akhmanova, A., and Galjart, N. (2003) *J. Neurosci.* **23,** 2655–2664
27. Aktories, K., Bärmann, M., Ohishi, I., Tsuyama, S., Jakobs, K. H., and Habermann, E. (1986) *Nature* **322,** 390–392
28. Vandekerckhove, J., Schering, B., Bärmann, M., and Aktories, K. (1988) *J. Biol. Chem.* **263,** 696–700
29. Mouritsen, O. G., and Zuckermann, M. J. (2004) *Lipids* **39,** 1101–1113
30. Christian, A. E., Haynes, M. P., Phillips, M. C., and Rothblat, G. H. (1997) *J. Lipid Res.* **38,** 2264–2272
31. Seveau, S., Bierne, H., Giroux, S., Prévost, M. C., and Cossart, P. (2004) *J. Cell Biol.* **166,** 743–753
32. Keller, P., and Simons, K. (1998) *J. Cell Biol.* **140,** 1357–1367
33. Giesemann, T., Jank, T., Gerhard, R., Maier, E., Just, I., Benz, R., and Aktories, K. (2006) *J. Biol. Chem.* **281,** 10808–10815
34. Shvartsman, D. E., Gutman, O., Tietz, A., and Henis, Y. I. (2006) *Traffic* **7,** 917–926
35. Lingwood, D., Binnington, B., Róg, T., Vattulainen, I., Grzybek, M., Coskun, U., Lingwood, C. A., and Simons, K. (2011) *Nat. Chem. Biol.* **7,** 260–262
36. Lingwood, D., and Simons, K. (2010) *Science* **327,** 46–50
37. Mayor, S., and Rao, M. (2004) *Traffic* **5,** 231–240
38. Quinn, P. J., and Wolf, C. (2009) *Biochim. Biophys. Acta* **1788,** 33–46
39. Danielsen, E. M., and Hansen, G. H. (2003) *Biochim. Biophys. Acta* **1617,** 1–9
40. Devaux, P. F., and Morris, R. (2004) *Traffic* **5,** 241–246
41. Grimmer, S., Spilsberg, B., Hanada, K., and Sandvig, K. (2006) *Traffic* **7,** 1243–1253
42. Harder, T., Scheiffele, P., Verkade, P., and Simons, K. (1998) *J. Cell Biol.* **141,** 929–942
43. Solomon, S., Masilamani, M., Rajendran, L., Bastmeyer, M., Stuermer, C. A., and Illges, H. (2002) *Immunobiology* **205,** 108–119
44. Zidovetzki, R., and Levitan, I. (2007) *Biochim. Biophys. Acta* **1768,** 1311–1324
45. Huttner, W. B., and Zimmerberg, J. (2001) *Curr. Opin. Cell Biol.* **13,** 478–484
46. McMahon, H. T., and Gallop, J. L. (2005) *Nature* **438,** 590–596
47. Doherty, G. J., and McMahon, H. T. (2009) *Annu. Rev. Biochem.* **78,** 857–902
48. Sandvig, K., Torgersen, M. L., Raa, H. A., and van Deurs, B. (2008) *Histochem. Cell Biol.* **129,** 267–276
49. Römer, W., Berland, L., Chambon, V., Gaus, K., Windschiegl, B., Tenza, D., Aly, M. R., Fraisier, V., Florent, J. C., Perrais, D., Lamaze, C., Raposo, G., Steinem, C., Sens, P., Bassereau, P., and Johannes, L. (2007) *Nature* **450,** 670–675
50. Römer, W., Pontani, L. L., Sorre, B., Rentero, C., Berland, L., Chambon, V., Lamaze, C., Bassereau, P., Sykes, C., Gaus, K., and Johannes, L. (2010) *Cell* **140,** 540–553
51. Safouane, M., Berland, L., Callan-Jones, A., Sorre, B., Römer, W., Johannes, L., Toombes, G. E., and Bassereau, P. (2010) *Traffic* **11,** 1519–1529
52. Ahmed, S., Goh, W. I., and Bu, W. (2010) *Semin. Cell Dev. Biol.* **21,** 350–356

53. Doherty, G. J., and McMahon, H. T. (2008) *Annu. Rev. Biophys.* **37,** 65–95
54. Hammond, A. T., Heberle, F. A., Baumgart, T., Holowka, D., Baird, B., and Feigenson, G. W. (2005) *Proc. Natl. Acad. Sci. U.S.A.* **102,** 6320–6325
55. Damm, E. M., Pelkmans, L., Kartenbeck, J., Mezzacasa, A., Kurzchalia, T., and Helenius, A. (2005) *J. Cell Biol.* **168,** 477–488
56. Hurley, J. H., Boura, E., Carlson, L. A., and Ró¿ycki, B. (2010) *Cell* **143,** 875–887
57. Stachowiak, J. C., Hayden, C. C., and Sasaki, D. Y. (2010) *Proc. Natl. Acad. Sci. U.S.A.* **107,** 7781–7786
58. Larive, R. M., Baisamy, L., Urbach, S., Coopman, P., and Bettache, N. (2010) *Biochim. Biophys. Acta* **1798,** 389–400